# Anatomy of the finite-length flux-tube and the flux-tube interaction in the DGL theory


Y. Koma[1] and M. Koma[2]

[1]*National Institute of Technology, Numazu College, Ooka 3600, Numazu 410-8501, Japan*

[2]*Research Center for Nuclear Physics (RCNP), Osaka University, Ibaraki, Osaka 567-0047, Japan*



**Abstract**

The dual Ginzburg-Landau (DGL) theory is one of the nonperturbative effective field theories of quantum chromodynamics (QCD). The DGL theory describes the QCD vacuum as a dual superconductor and possesses electric flux-tube solutions via the dual Meissner effect, which applies to the quark confinement mechanism. We demonstrate a powerful numerical method for solving the field equations in the DGL theory with U(1) dual gauge symmetry. An essential aspect of our method is to formulate the DGL theory on the dual lattice, which enables us to investigate any system composed of finite-length flux tubes in a systematic manner. We study the flux-tube interaction in terms of the shape of the Dirac string in the flux-tube solutions.


## 1 Introduction

The dual Ginzburg-Landau (DGL) theory is one of the nonperturbative effective field theories of QCD [1, 2, 3, 4]. The DGL theory describes the QCD vacuum as a dual superconductor [5, 6, 7] and possesses electric flux-tube solutions via the dual Meissner effect, which applies to the quark confinement mechanism. In ordinary superconductors, the vacuum is characterized by the Ginzburg–Landau (GL) parameter $\kappa$, defined as the ratio of the penetration depth to the coherence length. By analogy, it is natural to attempt to determine the corresponding GL parameter for the QCD vacuum. So far, numerous studies have been carried out to identify the type of vacuum (i.e., type-I or type-II dual superconductivity) by analyzing the field profiles of quark–antiquark systems in lattice QCD simulations. However, a definitive conclusion has yet to be reached, and the results remain inconclusive.

Part of the reason may be due to the difficulty of reducing numerical errors in the lattice QCD simulation, while another contributing factor may lie in the limitations of the analysis methods applied to the lattice data. For example, the field profiles of quark–antiquark systems obtained from lattice simulations have often been analyzed by fitting to simple exponential functions with negative exponents, from which the penetration depth or the coherence length is extracted. In most cases, however, the finite separation between the quark and the antiquark—an inherent feature of the simulations—is not adequately taken into account in such analyses. Since the numerical errors of lattice simulations are getting smaller, thanks not only to the increase of computer resources but also to the efficient numerical algorithms, it is quite important to use appropriate model functions for the analysis.

To make the discussion more concrete, we first present the Lagrangian of the DGL theory. The DGL theory with U(1) dual gauge symmetry is described by the Lagrangian

$$\mathcal{L} = -\frac{1}{4}\,{}^*F_{\mu\nu}{}^*F^{\mu\nu} + |(\partial_\mu + igB_\mu)\chi|^2 - \lambda\left(|\chi|^2 - v^2\right)^2, \tag{1}$$

where $B_\mu$ is the dual gauge field, $\chi$ is the monopole field carrying the magnetic charge $g$, and the dual field strength ${}^*F_{\mu\nu}$ includes the contribution from the Dirac string associated with an external quark–antiquark pair. The presence of the Dirac string leads to singular contributions to the field strength, which make the analysis technically involved. To avoid these divergences while solving the resulting nonlinear partial differential equations, it is necessary to impose boundary conditions on the fields with particular care. In many previous studies, this difficulty has effectively been circumvented by considering infinitely long, axially symmetric solutions. While such simplifications make the problem more tractable, they do not fully capture the features of realistic, finite-length flux-tube systems.

In this report, we present our recent results published in Ref. [8], demonstrating a powerful numerical method for solving the field equations in the DGL theory with U(1) dual gauge symmetry, including several updates to our previous work [9]. A key feature of our approach is the formulation of the DGL theory on a dual lattice, which allows us to systematically investigate systems composed of flux tubes of finite length and their interaction over a wide range of $\kappa$.

## 2 Formulation

The DGL action on an $L^3$ lattice is given by

$$S = \beta_g \sum_x \left[ \frac{1}{4} {}^*F_{\mu\nu}(x)^2 + \frac{\hat{m}_B^2}{2} (D_\mu \chi^\alpha(x))^2 + \frac{\hat{m}_B^2 \hat{m}_\chi^2}{8} \left( \chi^\alpha(x)^2 - 1 \right)^2 \right], \quad (2)$$

where $\chi(x) = \chi^1(x) + i\chi^2(x)$ ($\chi^\alpha \in \Re$), ${}^*F_{\mu\nu}(x) = (\partial \wedge B)_{\mu\nu}(x) - 2\pi\Sigma_{\mu\nu}(x)$ is the dual field strength and $D_\mu$ is the covariant derivative. The parameters $m_B$ and $m_\chi$ represent the masses of the dual gauge field and the monopole field, respectively. The magnetic charge $g$ is incorporated through the dual gauge coupling $\beta_g = 1/g^2$. All variables are dimensionless, and the physical scale can be recovered by using the lattice spacing $a \equiv \hat{m}_B/m_B$ if necessary. The field equations for the dual gauge field $B_\mu(x)$ and the monopole field $\chi^\alpha$ are given by

$$\frac{\partial S}{\partial B_\mu(x)} = \beta_g \Big( \sum_{\nu \neq \mu} [{}^*F_{\mu\nu}(x) + {}^*F_{\nu\mu}(x-\hat{\nu})] + \hat{m}_B^2 [\chi^\alpha(x)\chi^\alpha(x+\hat{\mu}) \sin B_\mu(x) + \epsilon_{\alpha\beta}\chi^\alpha(x)\chi^\beta(x+\hat{\mu}) \cos B_\mu(x)] \Big) = 0, \quad (3)$$

$$\frac{\partial S}{\partial \chi^\alpha(x)} = \beta_g \hat{m}_B^2 \Big( \sum_\mu [2\chi^\alpha(x) - \chi^\alpha(x+\hat{\mu}) \cos B_\mu(x) + \epsilon_{\alpha\beta}\chi^\beta(x+\hat{\mu}) \sin B_\mu(x) - \chi^\alpha(x-\hat{\mu}) \cos B_\mu(x-\hat{\mu})$$
$$- \epsilon_{\alpha\beta}\chi^\beta(x-\hat{\mu}) \sin B_\mu(x-\hat{\mu})] + \frac{\hat{m}_\chi^2}{2} \chi^\alpha(x)(\chi^\beta(x)^2 - 1) \Big) = 0 \,. \quad (4)$$

The task of solving coupled nonlinear partial differential equations for the field variables remains the same as in the ordinary discretization methods, but we do not need to struggle to set complicated boundary conditions for the field variables. For the quark-antiquark system, all we have to care about is specifying the locations of a quark and an antiquark as the ends of an open Dirac string $\Sigma_{\mu\nu}$. One of the most appealing features of the dual lattice formulation is that we can simply treat the Dirac string $\Sigma_{\mu\nu}$ in the dual field strength as integer values, which allows us to obtain the solution for various kinds of flux-tube systems without caring about the detailed boundary conditions of the field variables (see Fig.1). In this formulation, the positions of the point-like electric charges (quark and antiquark) are defined as the endpoints of the Dirac string. Since these endpoints are located within a lattice cell of volume $a^3$, these charges are effectively regularized.

Using the standard Newton-Raphson method, we always obtain the field configurations that minimize the energy of the system, independent of the choice of the Dirac string path.

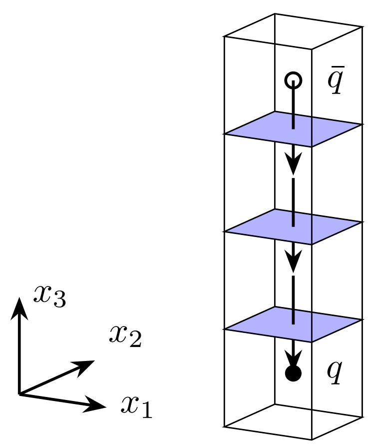


Figure 1: How to put the nonzero $\Sigma_{\mu\nu}$ for the quark-antiquark ($q\bar{q}$) system in $D = 3$ dimensions. This example is for the $R = 3$ case, where the $q\bar{q}$ axis is taken along the $x_3$-axis. The shaded part of $\Sigma_{12}$ is set to be $-N_q$, where $N_q \in \mathbb{Z}$ characterizes the scalar multiple of the electric charge $e$.

## 3 Numerical results

Let us demonstrate what the numerical solutions look like for the quark-antiquark system in $D = 3$ dimensions. We set $\hat{m}_B = \hat{m}_\chi = 0.50$ ($\kappa = 1.0$) and employ a $L^3 = 32^3$ lattice. After setting the Dirac string as in Fig. 1 with the trivial initial condition, we apply the Newton-Raphson method. To investigate the structure of the flux tube in more detail, we perform the Hodge decomposition of the dual field strength.

The decomposition is achieved by using the massless lattice Green function $G_L(x)$ in a finite volume, which satisfies

$$\Delta_L G_L(x-x') = \partial_\mu \partial'_\mu G_L(x-x') = -\delta_{xx'} + \frac{1}{L^D} \ , \tag{5}$$

where $\partial_\mu$ and $\partial'_\mu$ are forward and backward differences, respectively. The decomposed parts of the dual gauge field are then given by

$$B_\mu^{\mathrm{reg}}(x) = \sum_{x'} G_L(x-x')\partial'_\nu {}^*F_{\mu\nu}(x') \ , \tag{6}$$

$$B_\mu^{\mathrm{sing}}(x) = 2\pi \sum_{x'} G_L(x-x')\partial'_\nu \Sigma_{\mu\nu}(x') \ , \tag{7}$$

$$B_\mu^{\mathrm{red}}(x) = \sum_{x'} G_L(x-x')\partial_\mu(\partial'_\nu B_\nu(x')) \ . \tag{8}$$

The field strength then becomes

$$^*F_{\mu\nu} = (\partial \wedge B^{\mathrm{reg}})_{\mu\nu}(x) + 2\pi C_{\mu\nu}(x) \ , \tag{9}$$

where

$$C_{\mu\nu}(x) = -\epsilon_{\mu\nu\sigma}\partial'_\sigma \sum_{x'} G_L(x-x') j_0(x') \tag{10}$$

represents the Coulombic electric field.

The action can also be decomposed into two parts as

$$S = S_{\mathrm{coul}} + S_{\mathrm{sole}} \ , \tag{11}$$

where

$$S_{\mathrm{coul}} \equiv \beta_g \sum_x \frac{1}{4}[2\pi C_{\mu\nu}(x)]^2 \ , \tag{12}$$

$$S_{\mathrm{sole}} \equiv \beta_g \sum_x \left[ \frac{1}{4}[(\partial \wedge B^{\mathrm{reg}})_{\mu\nu}(x)]^2 + \frac{\hat{m}_B^2}{2}(D_\mu \chi^\alpha(x))^2 + \frac{\hat{m}_B^2 \hat{m}_\chi^2}{8}\left(\chi^\alpha(x)^2 - 1\right)^2 \right] . \tag{13}$$

The labels "coul" and "sole" refer to the Coulombic and the solenoidal parts, respectively, reflecting the structure of the resulting electric field profile (we will demonstrate this below).

We present the profile of the action density $s(x)$, where $S = \sum_x s(x)$ in Fig. 2 for the $R = 10$ case just on the midplane of the flux tube. The action density $s(x)$ can also be decomposed into two parts $s_{\mathrm{coul}}(x)$ and $s_{\mathrm{sole}}(x)$ as in Eqs.(12) and (13). We observe two sharp peaks at the location of the quark and antiquark in the Coulombic part, while a ridge structure between the quark and antiquark in the solenoidal part. Then, the sum of these two profiles gives the full action density. The height of the two sharp peaks themselves is not directly related to the interaction, but just reflects the self-energies of the quark and antiquark. The interaction occurs when the action density is *continuously connected* by positive values. When the quark and antiquark are close to each other, the tails of the two shape peaks overlap, yielding the Coulombic potential. As the quark and antiquark are separated, the overlap of the tails is reduced, and the ridge structure comes out of hiding. Since the height and width of the ridge are almost constant, which persists even when the quark and antiquark are separated further, there appears a linearly-rising potential with a constant positive slope.

The behavior of the action density is closely related to the profile of the electric field,

$$E_\mu = \frac{1}{2}\epsilon_{\mu\nu\rho} {}^*F_{\nu\rho} \ , \tag{14}$$

since the square of this quantity is a part of the action density. The electric field can also be decomposed into the Coulombic and the solenoidal parts. The Coulombic part of the electric field should behave as that around the electric dipole in electromagnetism. The solenoidal part is expected to behave similarly (but dual) to the magnetic field in and around a finite-length solenoid coil, which is the origin of its naming. In our case, the monopole supercurrent,

$$k_\mu = -\hat{m}_B^2[\chi^\alpha(x)\chi^\alpha(x+\hat{\mu})\sin B_\mu(x) + \epsilon_{\alpha\beta}\chi^\alpha(x)\chi^\beta(x+\hat{\mu})\cos B_\mu(x)] \ , \tag{15}$$

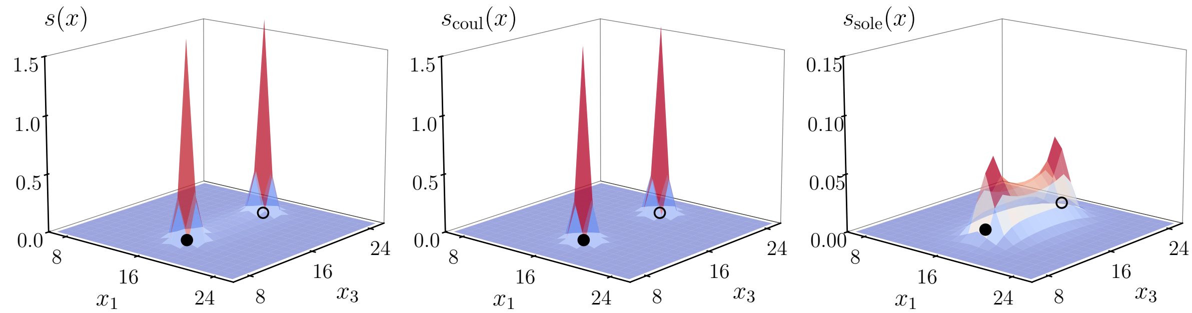


Figure 2: The profile of the full action density $s$ (left) with the Hodge decomposition, the Coulombic part $s_{\mathrm{coul}}$ (middle), and the solenoidal part $s_{\mathrm{sole}}$ (right), just on the median plane that the quark (the black-filled circle) and antiquark (the black-open circle) are placed for $\kappa = 1.0$ ($\hat{m}_B = \hat{m}_\chi = 0.50$) on the $L^3 = 32^3$ lattice, where the interquark distance is $R = 10$. Note that the vertical axis scale of the solenoidal part is one-tenth smaller than the others.

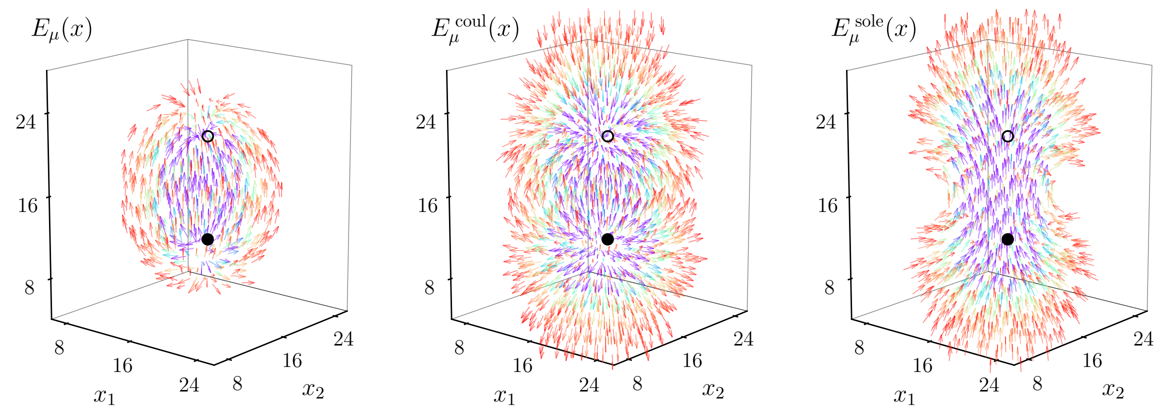


Figure 3: The profile of the full electric field $E_\mu$ (left) with the Hodge decomposition, the Coulombic part $E_\mu^{\mathrm{coul}}$ (middle), and the solenoidal part $E_\mu^{\mathrm{sole}}$ (right), for $\kappa = 1.0$ ($\hat{m}_B = \hat{m}_\chi = 0.50$) on the $L^3 = 32^3$ lattice, where the interquark distance is $R = 10$, and the locations of the quark and antiquark are specified by the black-filled and black-open circles, respectively. The values for $|E_\mu| \geq 0.004$ are displayed, and the strength is represented by a color scale, with violet indicating higher magnitudes.

acts as the circular current.

In Fig. 3, we show the electric field $E_\mu(x)$ with the Hodge decomposition. Since $R = 10$ corresponds to 5.0 $[1/\mathrm{m_B}]$ for $\hat{m}_B = 0.50$, one may naively expect a tube-like structure with the ratio, length : diameter = 5 : 2, however, the profile of the full electric field in Fig. 3 (left) rather looks like a sphere. In this sense, the naming, such as the "flux tube" which evokes translational invariance of the profile, may not always be appropriate, though we use this term to express the solution throughout this paper. To observe a thin tube-like structure for the electric field, the $\kappa$ should be larger, or the length $R$ should be unrealistically longer compared to the penetration depth. In fact, the penetration depth alone does not characterize the width of the electric-field profile properly when $\kappa$ is finite. Since the electric field is suppressed exponentially beyond the distance of the coherence length, it is reasonable to think that the width of the electric-field profile is roughly given by the sum of the coherence length and the penetration depth. For the $\kappa = 1$ case, the width will then be twice the penetration depth, so that the above naive ratio should be modified to length : diameter = 5 : 4, which may be consistent with the appearance.

Even if the full electric-field profile does not show a tube-like structure, it is not the same as the Coulombic field, since the full electric field is given by the sum of the real Coulombic field in Fig. 3 (middle) and the solenoidal field in Fig. 3 (right). The solenoidal part plays a role in cancelling the Coulombic field in the outer region, which, at the same time, enhances the electric field in the inner region around the Dirac string. In Fig. 4, we show the profiles of the circulating monopole supercurrent $k_\mu(x)$ and the monopole field $\phi(x) = |\chi(x)|$. In the region where the electric field has a large value, $\phi(x)$ necessarily takes a value smaller than one, indicating

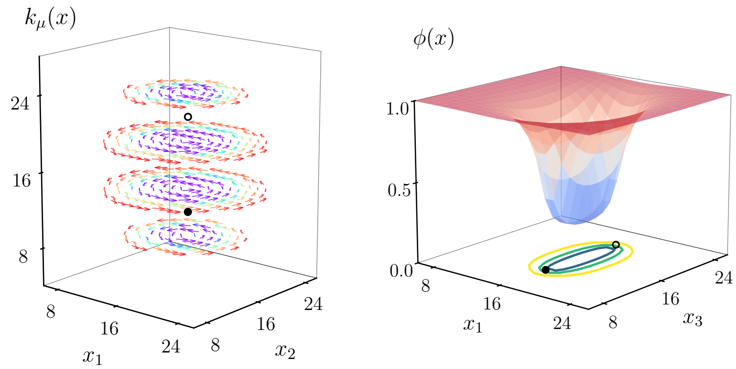


Figure 4: The profiles of the monopole supercurrent $k_\mu(x)$(left) and the monopole field $\phi(x) = |\chi(x)|$(right) for $\kappa = 1.0$ ($\hat{m}_B = \hat{m}_\chi = 0.50$) on the $L^3 = 32^3$ lattice, where the interquark distance is $R = 10$, and the locations of the quark and antiquark are specified by the black-filled and black-open circles, respectively. The values with $|k_\mu| \geq 0.001$ on the four selected planes are displayed, and the strength is represented by a color scale, with violet indicating higher magnitudes.

the melting of vacuum condensate.

The shape of the flux-tube solution may depend on the path of how the Dirac string is put. As we will show below, however, the iteration process always tries to find a minimum energy configuration of the fields, so that the final path of the Dirac string is not always the same as the initial one. During the iteration process of the Newton-Raphson method, the phase of the monopole field or the redundant part of the dual gauge field can become multi-valued, which generates a new set of Dirac strings. This happens when the flux tube along the original Dirac string $\Sigma_{\mu\nu}$ is energetically unstable. The sum of the original and the generated Dirac strings then determines the final Dirac string that is responsible for the flux-tube solution.

In practice, the location of the final Dirac string in $D = 3$ dimensions can be identified by the following procedure. Firstly, we identify the total winding number of the dual gauge field, including the contribution from the phase of the monopole field $\eta(x) = \tan^{-1}(\chi^2(x)/\chi^1(x)) \in [-\pi, \pi)$ by

$$n_\mu(x) \equiv \mathrm{floor}(\frac{B_\mu(x) + \partial_\mu \eta(x) + 5\pi}{2\pi}) - 2 \, , \tag{16}$$

where the shift of $5\pi$ is just for technical reasons, and the function floor($arg$) is assumed to return the greatest integer value less than or equal to $arg$. When $n_\mu \neq 0$ the closed Dirac string is generated by

$$\Sigma^{\mathrm{closed}}_{\mu\nu}(x) = (\partial \wedge n)_{\mu\nu}(x) \, , \tag{17}$$

which satisfies $\sum_x \Sigma^{\mathrm{closed}}_{\mu\nu}(x) = 0$ regardless of the choice of $\mu\nu$ planes. Secondly, we extract the remnant of the dual gauge field by

$$B^{\mathrm{rem}}_\mu(x) = B_\mu(x) - 2\pi n_\mu(x) \, , \tag{18}$$

which allows us to compute the final location of the Dirac string by

$$\begin{aligned} \Sigma^{\mathrm{final}}_{\mu\nu}(x) &= \mathrm{floor}(\frac{(\partial \wedge B^{\mathrm{rem}})_{\mu\nu}(x) - 2\pi C_{\mu\nu}(x) + 5\pi}{2\pi}) - 2 \\ &= \Sigma_{\mu\nu}(x) + \Sigma^{\mathrm{closed}}_{\mu\nu}(x) \, , \end{aligned} \tag{19}$$

where the subtraction of the Coulombic electric field $C_{\mu\nu}$ is crucial when a finite-length flux tube with higher charges $N_q \geq 2$ is investigated, since the large value of the electric field proportional to $N_q$ often leads to the wrong integer value which is not related to the string singularity. Note that the location of the Dirac string identified by

$$\mathrm{floor}(\frac{(\partial \wedge B)_{\mu\nu}(x) - 2\pi C_{\mu\nu}(x) + 5\pi}{2\pi}) - 2 \, , \tag{20}$$

is the same as the original Dirac string $\Sigma_{\mu\nu}$, so that the cancellation of the Dirac string occurs in the field strength, leaving the Coulombic term as in Eq. (9).

Let us see a typical example of the generation of the closed string on a $32^3$ lattice with $\hat{m}_B = \hat{m}_\chi = 0.50$. We first put the Dirac string along the side of a cube as shown in Fig. 5 (left) and start the Newton-Raphson method, where the ending and starting points of the string, $(x_1, x_2, x_3) = (13.5, 13.5, 13.5)$ and $(19.5, 19.5, 19.5)$,

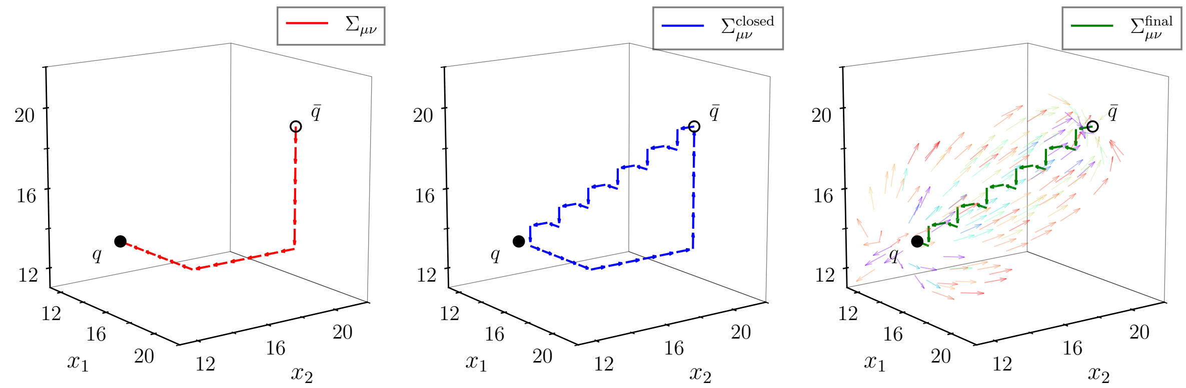


Figure 5: The vector representation of the original Dirac string $\Sigma_{\mu\nu}$ (left), the generated closed Dirac string $\Sigma^{\rm closed}_{\mu\nu}$ (middle), and the final Dirac string $\Sigma^{\rm final}_{\mu\nu}$ (right), where the ending and starting points of the string, $(x_1, x_2, x_3) = (13.5, 13.5, 13.5)$ and $(19.5, 19.5, 19.5)$, correspond to the quark source and the antiquark sink, respectively. The profile of the electric field $E_\mu$ is also plotted with $\Sigma^{\rm final}_{\mu\nu}$.

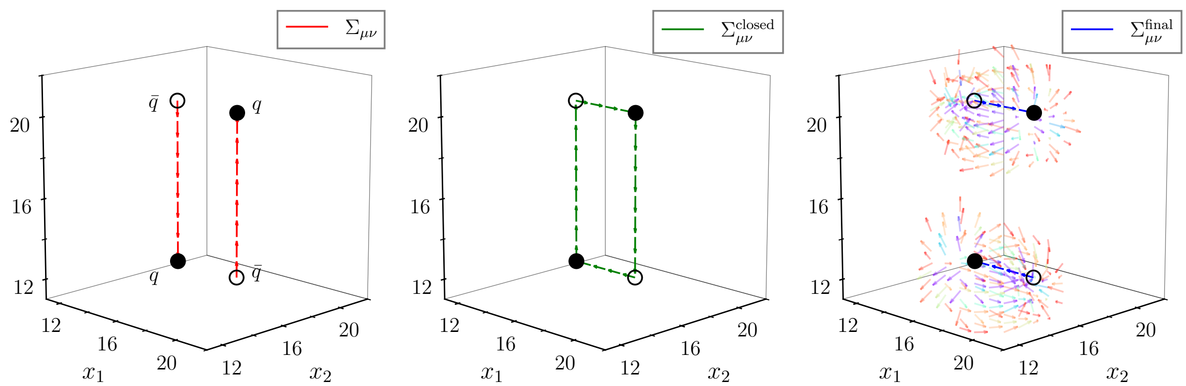


Figure 6: The initial position of the Dirac strings (left), the induced closed Dirac String(middle), and the resulting flux tube solution (right). The final position of the Dirac string is determined only by the energy minimum condition. End points of the initial Dirac stings are act as the boundary condition of the field equations.

correspond to the quark source and the antiquark sink, respectively. The convergence criterion is $\epsilon = 10^{-6}$. Note that we always compute $\frac{1}{2}\epsilon_{\mu\nu\rho}\Sigma_{\nu\rho}(x)$ etc. for identifying the string in the $\mu$ direction. Once the field equations are satisfied, we evaluate Eq. (17) and obtain the string as shown in Fig. 5 (middle). The final string in Eq. (19) has the structure as shown in Fig. 5 (right), where the corresponding electric field $E_\mu(x)$ is also plotted. Clearly, the location of the Dirac string is different from that of the original one, and the flux tube is formed along the final Dirac string.

It may be interesting to see what happens if two open Dirac strings are placed in parallel with the opposite direction. On $32^3$ lattice with $\hat{m}_B = \hat{m}_\chi = 0.50$, we put the two original Dirac strings along the $x_3$-axis from $(x_1, x_2, x_3) = (14.5, 16.5, 12.5)$ to $(14.5, 16.5, 20.5)$ and from $(18.5, 16.5, 20.5)$ to $(18.5, 16.5, 12.5)$. We then obtain the result as shown in Fig. 6, where the original Dirac string (left), the generated closed Dirac string (middle), and the final Dirac string (right) are plotted. We find that the sum of the original Dirac string and the generated closed Dirac string leads to the final Dirac string. If we only look at the original and the final Dirac strings, we may interpret this result as an occurrence of the *string flip*.

In Fig. 7, we show the final profile of the Dirac string as a representative of the flux-tube solution for $R = 56$ $(22.4\ [1/\mathrm{m_B}])$ with the distance between two original Dirac strings $X = 8$ $(3.2\ [1/\mathrm{m_B}])$, where some selected cross sections of the monopole field $\phi = |\chi|$ are also presented. We find that the two Dirac strings are bent inwards with each other for $\kappa = 0.50$ (left), and outwards for $\kappa = 1.5$ (right), which clearly indicates the appearance of attractive and repulsive forces between the two flux tubes, respectively. On the other hand, the two Dirac strings remain straight as in the original setting for $\kappa = 1.0$ (middle), as if there is no interaction. From the contour of the monopole field, we may learn that the total energy cost for digging holes in the monopole field

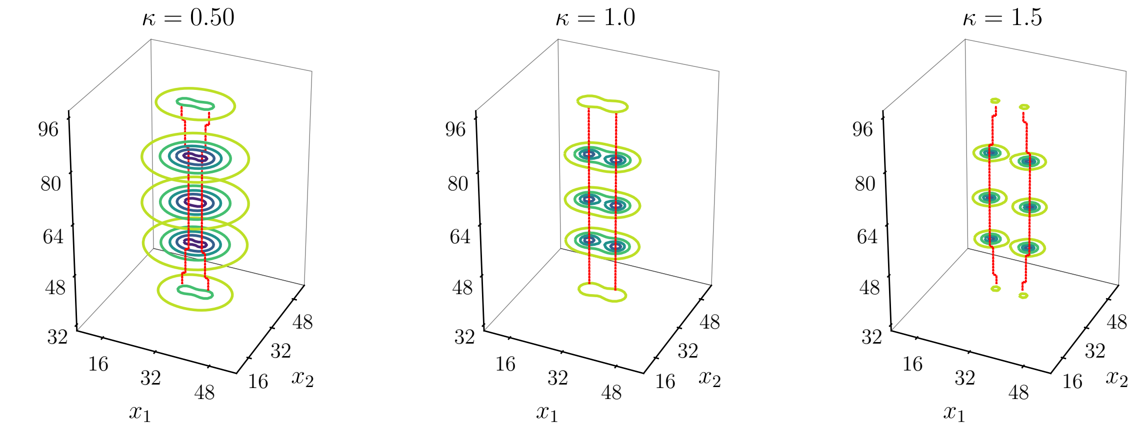


Figure 7: The profile of the final Dirac string for the two-flux-tube system ($R = 56$, $X = 8$) with the contours of the monopole field $\phi = |\chi|$ at $x_3 = 35, 51, 64, 78, 94$. The values of the contour lines from outer to inner are $\phi = 0.9, 0.7, 0.5, 0.3, 0.1$. We set $\hat{m}_B = 0.40$ and $L^2 L_3 = 64^2 128$.

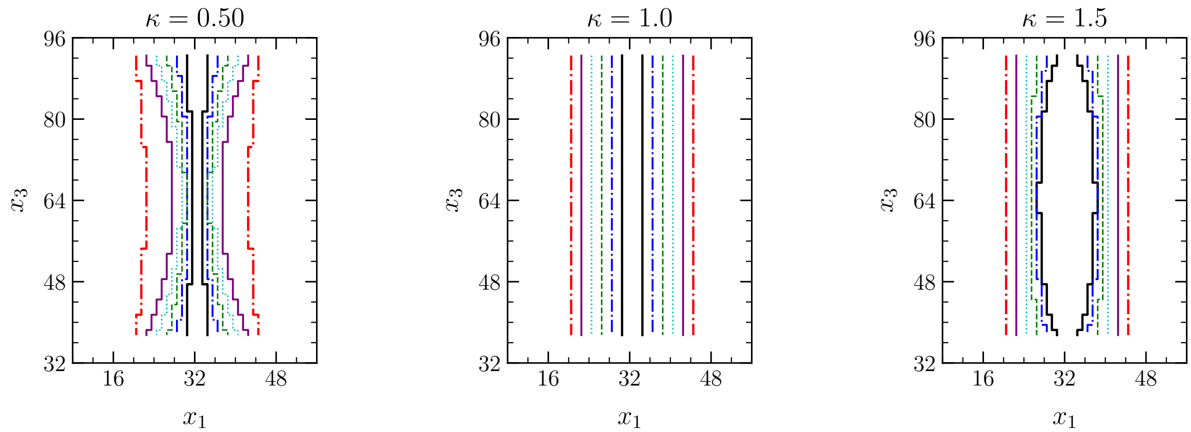


Figure 8: The profile of the final Dirac strings for the two-flux-tube system with $R = 56$ with various original separations $X = 4, 8, 12, 16, 20, 24$, where the same line-type and color are the pair for each $X$ ($X = 24$ is the outermost pair). The 3D profile for $X = 8$ is shown in Fig. 7.

along the path of the Dirac string is related to the final shape of the Dirac string, such that a single hole is preferable for $\kappa = 0.50$ even though the hole diameter is enlarged, while double holes are preferable for $\kappa = 1.5$. There is no such preference for $\kappa = 1.0$ in terms of the energy cost, so that the original Dirac strings can remain intact.

The interaction of the two flux tubes can further be investigated by changing the distance $X$ as shown in Fig. 8. This plot indicates that for $\kappa = 0.50$ the two flux tubes are eager to be combined to create a single flux tube as they are closer, while for $\kappa = 1.5$ the two flux tubes are eager to be apart from each other and can be independent once they are separated enough. For $\kappa = 1.0$, it is clear that the two Dirac strings remain straight regardless of the distance $X$. Another feature of the flux-tube interaction suggested from these figures is that a flux tube has a finite interaction range depending on $\kappa$; the final shape of the flux tubes may not be determined solely by the global minimum of the energy.

## 4 Summary

In this report, we have demonstrated a numerical method for solving the field equations in the dual Ginzburg-Landau (DGL) theory on a dual lattice [8]. A key feature of this formulation is the simple treatment of the Dirac string as an integer-valued variable, which allows us to investigate flux-tube profiles without imposing complicated boundary conditions. We have presented numerical solutions for finite-length flux tubes and analyzed their structure through the Hodge decomposition. The decomposition into Coulombic and solenoidal components provides a clear physical picture of the flux-tube formation, where the solenoidal field plays a crucial role in confining the electric flux. Furthermore, we have studied the interaction between flux tubes by examining systems with multiple Dirac strings. The numerical results clearly show that the interaction depends on the value of the Ginzburg-Landau parameter $\kappa$: attraction for $\kappa < 1$, repulsion for $\kappa > 1$, and marginal behavior near $\kappa = 1$. The deformation and rearrangement of the Dirac strings indicate that the flux-tube configurations are dynamically determined through energy minimization. These results demonstrate that the present method provides a powerful and flexible framework for investigating nonperturbative properties of the QCD vacuum, including the structure and interaction of flux tubes over a wide range of $\kappa$.

## References


[1] T. Suzuki, Prog. Theor. Phys. **80**, 929 (1988) doi:10.1143/PTP.80.929

[2] S. Maedan and T. Suzuki, Prog. Theor. Phys. **81**, 229-240 (1989)

[3] H. Suganuma, S. Sasaki and H. Toki, Nucl. Phys. B **435**, 207-240 (1995) [arXiv:hep-ph/9312350 [hep-ph]].

[4] S. Sasaki, H. Suganuma and H. Toki, Prog. Theor. Phys. **94**, 373-384 (1995)

[5] Y. Nambu, Phys. Rev. D **10**, 4262 (1974)

[6] S. Mandelstam, Phys. Rept. **23**, 245-249 (1976)

[7] G. 't Hooft, Gauge Fields with Unified Weak, Electro- magnetic, and Strong Interactions, in 1975 High-Energy Particle Physics Divisional Conference of EPS (includes 8th biennial conf on Elem. Particles) (1975).

[8] Y. Koma and M. Koma, Phys. Rev. D **112**, 094511 (2025) [arXiv:2510.12168 [hep-lat]].

[9] Y. Koma, E.-M. Ilgenfritz, T. Suzuki and H. Toki, Phys. Rev. D **64**, 014015 (2001) [arXiv:hep-ph/0011165 [hep-ph]].